Azide Reduces the Hydrophobic Barrier of the Bacteriorhodopsin Proton Channel

Heinz-Jürgen Steinhoff,* Matthias Pfeiffer,# Thomas Rink,* Oliver Burlon,* Matthias Kurz,* Jens Riesle,# Ester Heuberger,# Klaus Gerwert,* and Dieter Oesterhelt#

*Lehrstuhl für Biophysik, Ruhr-Universität Bochum, 44780 Bochum, Germany, and #Max-Planck-Institut für Biochemie, Am Klopferspitz 18 a, 82152 Martinsried, Germany

ABSTRACT The sensitivity of a nitroxide spin label to the polarity of its environment has been used to estimate the hydrophobic barrier of the proton channel of the transmembrane proton pump bacteriorhodopsin. By means of site-specific mutagenesis, single cysteine residues were introduced at 10 positions located at the protein surface, in the protein interior, and along the proton pathway. After reaction with a methanethiosulfonate spin label, the principle values of the hyperfine tensor A and the g-tensor were determined from electron paramagnetic resonance spectra measured at 170 K. The shape of the hydrophobic barrier of the proton channel is characterized in terms of a polarity index, ΔA, determined from the variation of the hyperfine coupling constant A_{zz}. The maximum of the hydrophobic barrier is found to be close to the retinal chromophore in the proton uptake pathway. The effect of the asymmetric distribution of charged and polar residues in the proton release and uptake pathways is clearly reflected in the behavior of the hydrophobic barrier. The presence of azide reduces the barrier height of both the cytoplasmic and extracellular channels. This finding supports the view of azide and other weakly acidic anions as catalysts for the formation of hydrogen-bonded networks in proton pathways of proteins.

INTRODUCTION

The membrane protein bacteriorhodopsin (BR) is a model system of a light-driven proton pump that is ideally suited to study proton transport mechanisms in proteins. BR is the integral protein of the purple membrane of *Halobacterium salinarum* (for reviews see, e.g., Lanyi, 1993; Oesterhelt, 1998). Seven transmembrane helices enclose the binding pocket for the all-*trans* retinal chromophore, which is bound to K216 via a protonated Schiff base. Absorption of a photon by the retinal induces the 13-*cis* isomerization, which initiates the catalytic cycle with the spectroscopically characterized intermediates J, K, L, M, N, O, and the initial state BR. Crucial events during the catalytic cycle are the deprotonation of the Schiff base during the L to M transition, which is accompanied by a protonation of D85 and the appearance of a proton at the extracellular surface. The Schiff base is reprotonated during the M to N transition from the proton donor D96, which is finally reprotonated from the cytoplasm during the recovery to the BR initial state.

Several cavities in the molecular structure large enough to be filled with water were initially suggested from electron diffraction data (Grigorieff et al., 1996; Kimura et al., 1997). Neutron diffraction data support the presence of at least seven water molecules in the extracellular (EC) and cytoplasmic (CP) channels (Hauss et al., 1997). Three ordered water molecules could be resolved by x-ray diffraction experiments and a hydrogen-bonded network including water molecules and several polar residues could be refined in the EC channel (Lücke et al., 1998). Hydrogen-bonded networks seem to be essential to facilitate fast proton transfer in both the EC and CP parts of the proton pathways (Cao et al., 1991; Varo and Lanyi, 1991; Tittor et al., 1994; Le Coutre et al., 1995; Brown et al., 1995; Rammelsberg et al., 1998; Wikström, 1998). The existence of such networks in both the EC and CP channels was first concluded from FTIR studies (Le Coutre et al., 1995; Hatanaka et al., 1997; Rammelsberg et al., 1998). Strikingly, the properties of this hydrogen-bonded system seem to be modulated by the presence of weakly acidic anions like azide, cyanate, and formate. The reprotonation rate of the Schiff base of the defective proton pump with Asp-96 mutated to Asn, D96N, is even enhanced compared to that of the wild-type protein after the addition of azide (Tittor et al., 1989). The effect of azide was proposed to be due to an influence on the hydrogen-bonded system in both the EC and CP channels. Thus, it seems worthwhile to study the shape of the hydrophobic barrier the proton has to overcome on its path through the protein in the presence and absence of azide.

In the present report we have used the sensitivity of the electron paramagnetic resonance (EPR) spectra of nitroxides toward the environmental polarity to characterize the behavior of the hydrophobic barrier in BR (Griffith et al., 1974; Earle et al., 1994). Site-specific mutagenesis was used to introduce single cysteines at selected positions in the protein interior and along the proton channel. The cysteines were reacted with a specific methanethiosulfonate spin label. This method of site-directed spin labeling (for reviews see, e.g., Hubbell and Altenbach, 1994; Hubbell et al., 1996) was used in the past to determine the identity and orienta-

Received for publication 28 August 1998 and in final form 28 January 1999.

Address reprint requests to Dr. Heinz J. Steinhoff, Lehrstuhl für Biophysik, Ruhr-Universität Bochum, Universitätstrasse 150, D-44780 Bochum, Germany. Tel.: 49-234-700-4463; Fax: 49-234-709-4626; E-mail: hjs@bph.ruhr-uni-bochum.de.

0006-3495/99/05/2702/09 $2.00

tion of secondary structure of protein domains, the topography of polypeptide chains with respect to the membrane solution interface, and to resolve conformational changes in space and time in a millisecond time range (Steinhoff et al., 1994; Rink et al., 1997). This technique is applied here to study the polarity profile along the BR proton pathway in the presence and absence of azide. For this purpose, the effect of the environment on the ^{14}N coupling constant, A_{zz}, is determined from frozen samples ($T < 170$ K) and characterized in terms of a polarity index ΔA according to the method developed by Griffith and co-workers (1974).

MATERIALS AND METHODS

Mutagenesis, expression, and spin labeling

Site-specific mutants of bacteriorhodopsin were prepared according to Ferrando et al. (1993). The codon of any requested position was changed to TGC coding for cysteine by means of site-directed mutagenesis by overlap extension. The PCR product was cloned in the shuttle vector pUS-Mev (Schweiger, 1996). This vector is a derivative of the commercial vector pBluescript SK$^-$ containing the *Hin*dIII-*Xho*I fragment from the vector pWL102 mediating resistance against mevinoline (Lam and Doolittle, 1989) and the *Bam*HI-*Hin*dIII fragment from pEF191 with the coding gene for bacterio-opsin (Ferrando et al., 1993). Homologous expression was followed by transformation of the *H. salinarum* strain SNOB, which is a bacterio-opsin gene-deficient derivative of the strain S9 (S9 without bop). Mutated proteins were isolated as purple membrane sheets according to Oesterhelt and Stoeckenius (1974). For confirmation of the *H. salinarum* transformants total DNA was isolated, the bacterio-opsin gene was amplified by PCR, and sequenced.

The spin label (1-oxyl-2,2,5,5-tetramethylpyrroline-3-methyl)methanethiosulfonate (MTSSL) (Reanal, Budapest, Hungary) was covalently attached to the cysteines of the membrane-bound BR mutants to yield the spin label side chain R1 (Fig. 1). For this purpose, 10 μl of a solution of 100 mM MTSSL in DMSO was added to a 2.5-ml suspension of membranes in 0.1 M phosphate buffer, 0.1 M NaCl, pH 7.4, resulting in a spin label/BR ratio of 10:1. DMSO (40%) was added to partially unfold the protein and provide efficient accessibility to the internally located cysteines (Oesterhelt et al., 1973). The samples were then incubated at room temperature for 12 h. Afterward, the noncovalently bound spin label and the DMSO were removed by washing the membrane pellet to refold the protein. Inspection of the absorbance spectra and the photocycle kinetics shows that the partial unfolding by DMSO was completely reversible. The labeled cysteine/BR ratio estimated from double integration of the EPR spectra and optical spectroscopy of BR was found to be close to one for all samples.

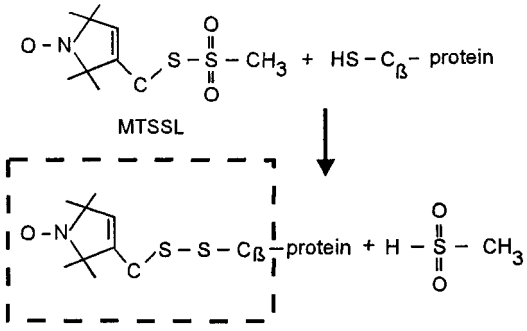

FIGURE 1 Reaction of the MTS spin label to generate the nitroxide side chain R1.

EPR and optical measurements

EPR spectra were recorded with a home-made X-band EPR spectrometer equipped with an H_{103} cavity (AEG) and a Bruker B-NM 12 B-field meter. Spin-labeled purple membrane was suspended in 0.1 M phosphate buffer, pH 7.4, 0.1 M NaCl, and loaded into EPR quartz capillaries (50 μl) at a final BR concentration of 200–500 μM. Spectra were taken at 170 K with a modulation amplitude of 1.8 G. After analog-to-12-bit digital conversion, the data were processed in a personal computer. EPR spectra simulations were performed according to the method described by Steinhoff (1988).

For power saturation experiments in the presence of oxygen or chromium oxalate (CROX) the samples were loaded into gas-permeable TPX capillaries (Jagmar Ltd., Kraków, Poland). The samples were deoxygenated by passing nitrogen around the sample capillary. Saturation curves were determined from the peak-peak amplitudes of the center line measured at seven different incident microwave power levels in the range from 0.5 to 80 mW. The saturation behavior of the samples was parametrized by the quantity $P_{1/2}$, which is defined as the power level of the incident radiation at which the amplitude of the saturated line is half of the amplitude in absence of saturation. Values for this parameter were calculated from fitting of the function

$$A(P) = I\sqrt{P}\cdot(1 + (2^{1/\epsilon} - 1)\cdot P/P_{1/2})^{-\epsilon}$$

to the experimental amplitudes $A(P)$ according to the method of Altenbach et al., (1994a). The scaling factor I and the measure of the saturation homogeneity ϵ are adjustable parameters. The quantity $\Delta P_{1/2}$ is calculated from the difference in $P_{1/2}$ values in the presence and absence of the relaxing agent. The $\Delta P_{1/2}$ values are divided by the peak-peak center line width and normalized by the same quantity of a DPPH standard sample to obtain the dimensionless accessibility parameter Π.

Transient absorbance changes of samples with an optical density, $OD_{568} = 0.8$, were recorded at 11 wavelengths between 405 and 665 nm (405, 415, 450, 470, 488, 515, 550, 580, 605, 635, and 665 nm) using a home-made optical setup. Depending on the signal-to-noise ratio the transient signals determined in the visible and the EPR spectral changes were sampled between 50 and 2000 times. The bandwidth of the amplifier was reduced to a time constant of 16 μs. The repetition rate was set between 0.5 and 0.06 s^{-1}, depending on the photocycle duration of the respective mutant. The time courses of the transient optical absorbance changes were analyzed by a global fitting procedure (Rink et al., 1997).

FT-Raman experiments

Near-infrared excitation at 1064 nm was performed with an Nd-Yag laser (ADLAS) with 350 mW laser power. Raman scattered light was measured with a Bruker FRA-Raman module. The BR samples were filled in quartz sample capillaries. Light adaptation was achieved by 10-min illumination with a 250 W tungsten lamp equipped with a heat filter. One hundred Raman spectra were accumulated within a sample time of 2.5 min.

RESULTS

Functional and structural properties of the spin-labeled cysteine mutants

Fig. 2 shows a model of the bacteriorhodopsin molecule according to the data of Grigorieff et al. (1996). Spin labels were located at the indicated positions within the loops at the cytoplasmic and extracellular surface of the protein and within the protein interior, mainly in the cytoplasmic part. Residues T170R1, E166R1, and V167R1 are located at the cytoplasmic end of helix F. The nitroxide side chain of T170R1 and E166R1 are oriented toward helix G, that of V167R1 points toward helix B into the entrance of the CP

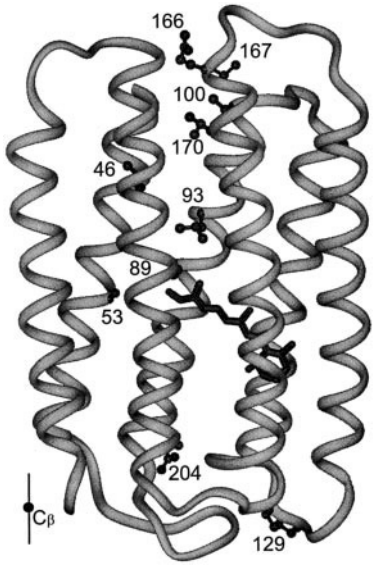

FIGURE 2 Structural model of bacteriorhodopsin according to the data of Grigorieff et al. (1996). The spin-labeled residues, the proton donor D96, and the chromophore retinal are indicated. The bar in the lower left corner illustrates the maximum vertical (i.e., parallel to the helix axes) deviation of the NO-group from the C_β of the respective residue.

channel (Grigorieff et al., 1996; Essen et al., 1998; Pfeiffer et al., 1999). Residue L100R1 in helix C provides a side chain location one α-helical turn apart from that of the proton donor D96. Residues T46R1 and L93R1 are located on the proton pathway between the proton donor D96 and the Schiff base. The side chains of A53R1 and T89R1 are found close to the Schiff base at helices B and C. Residues E204R1 and K129R1 provide side chain positions in the extracellular part of the molecule at the extracellular end of helix G and in the D-E loop.

Due to the different structure and flexibility of the nitroxide side chain, its orientation may deviate from that of the respective native side chain. Using the molecular modeling tools of the program package InsightII (Biosym) different orientations of an attached nitroxide with respect to the α-helix were constructed by variation of the side chain torsional angles. The distance between the projections of the N-O group and of the C_β onto the helix axis were determined. The maximum distance was found to be <0.35 nm in either direction along the helix (cf. Fig. 2).

A potential difficulty in all spin labeling experiments is the perturbation introduced by the label itself. It has to be checked whether the structure and thus the function of the protein with the spin label attached is retained. To answer this question we analyzed the photocycle of bacteriorhodopsin, since this is a sensitive measure of the integrity of the BR structure. The photocycle was followed at 11 wavelengths in the range from 405 to 665 nm and a multiexponential function was fitted to the transients. With the exception of T170R1, three exponentials were found to be sufficient to describe the decay of the M intermediate to the BR initial state. The time constants and the corresponding relative amplitudes determined for 415 nm are given in Table 1. The nomenclature of the time constants is given according to Hessling et al. (1993). The time constants τ_3 and τ_4 describe the decay of M. Formation of the N and O intermediates is described by τ_4, their decay by τ_3 and τ_6. Half-times of the M-decay similar to those of the wild type are found for the BR mutants with the spin labels attached within the loop regions, E166R1 and K129R1, and for T46R1 and L93 R1. The largest delay of the M decay is found for T89R1, where $t_{1/2}$ amounts to fivefold the corresponding value of the wild type. In turn, the spin labels attached to positions 100, 167 and 170 seem to predispose a fast proton transfer from D96 to the Schiff base as seen from the short lifetimes of M. Thus, effects of the spin labeling on the photocycle time are visible; however, the nitroxides in the proton channel do not seriously restrict the reprotonation of the Schiff base. The comparison with the values of the wild-type protein shows that the BR recovery time τ_6 is generally increased by the introduction of the spin labeled side chain. This is pronounced for the mutation at positions 93 and 170. A forth time constant of 1.3 s is necessary to describe the recovery of the BR initial state of T170R1. The amplitude spectrum of mutant L93R1 shows the accumulation of a blue-shifted O-like intermediate which, in contrast to the wild-type O intermediate, decays with τ_6. Accumulation of O is also observed for the mutants K129R1 and E204R1.

The influence of the nitroxide side chain on the configurational changes of the retinal was additionally studied for the mutants in its close vicinity, A53R1, T89R1, and L93R1. The light-to-dark adaptation process in the absence of undesired photo reactions (Schulte and Bradley, 1995) was analyzed with Raman spectroscopy. The change of the Raman scattering intensity of the ethylenic mode band of the all-*trans* (1526 cm^{-1}) isomer in the dark and after light

TABLE 1 Time constants and amplitudes of the M-decay resulting from a three-exponential fitting of the absorbance transients measured at 11 different wavelengths in the visible spectrum

Sample	τ_4/ms	τ_3/ms	τ_6/ms	$t_{1/2}$/*ms*
Wild type	2.2 (33%)	7.0 (67%)	18 (0%)	3.2
T46R1	5.1 (85%)	42 (15%)	290 (0%)	4.3
A53R1	11.4 (100%)	49 (5%)	207 (−5%)	7.8
T89R1	6.5 (28%)	38 (72%)	127 (0%)	15.8
L93R1	5.6 (83%)	44 (17%)	651 (0%)	4.9
L100R1	0.8 (100%)	30 (5%)	250 (−5%)	0.6
K129R1	2.4 (56%)	8.8 (38%)	78 (6%)	2.9
E166R1	1.8 (70%)	12 (27%)	83 (3%)	1.9
V167R1	1.1 (85%)	4.0 (14%)	74 (0%)	0.9
T170R1*	1.0 (84%)	11 (19%)	110 (2%)	0.9
E204R1	9.0 (50%)	33 (50%)	—	11.2

The respective relative amplitudes of the exponential functions that describe the transients at 415 nm are given in brackets. To facilitate comparison with published data, half-times of the M decay are given in the last column.

*A fourth time constant is required to fit the recovery to the BR initial state: 1300 ms (−5%).

adaptation was used to calculate the 13-*cis*-15-*syn* to all-*trans* ratio in the dark-adapted protein. This ratio was found to be close to 1 for wild-type, L93R1, and for A53R1. In contrast, the isomer equilibrium of the retinal in the dark-adapted mutant T89R1 is completely shifted to the 13-*cis*-15-*syn* isomer. The light-to-dark adaptation is accelerated compared to the wild type and could only be followed at low temperatures. We found a relaxation time of <10 min at 263 K compared to 27 min at 293 K for the wild-type protein. In contrast, the lifetime of the all-*trans* isomer is prolonged in the A53R1 mutant.

The results on the kinetics of the photocycle and the light-to-dark adaptation reveal that the overall structure and function of the protein seems to be retained, even for the mutants with the nitroxide side chain in close vicinity of the retinal. No evidence for a considerable unfolding is present, thus the structure of the proton channel is considered to be integer with respect to its dielectric and hydrophobic properties.

Mobility of the nitroxide side chains

The shape of the EPR spectra measured at room temperature (Fig. 3) reveals the degree of the nitroxide mobility, which depends on the protein structure in the vicinity of the spin label binding site (Mchaourab et al., 1996; Steinhoff and Hubbell, 1996). Comparably small apparent hyperfine splitting and small linewidths of the center line were found for the spin labels attached to K129C and E166C. These residues are located in the D-E loop and at the cytoplasmic end of helix F, respectively. In loop regions and helix termini the interaction of the spin label side chain with neighboring side chains and backbone atoms is small, thus the reorientational motion of the nitroxide is hardly restricted. Additionally, loops and helix termini themselves show some degree of flexibility, which may contribute to the observed side chain dynamics. Consequently, the linewidth and the hyperfine splitting are small. The spectra of the nitroxides attached to the residues T46C, A53C, T89C, L93C, T170C, and E204C exhibit strong motional restrictions in agreement with their location in the interior of the protein. This is also true for the spin labels of L100R1 and V167R1. This is evidence for a structured environment in the vicinity of the binding sites where the helix connects to the loop. This finding agrees nicely with the structural model (Essen et al., 1998).

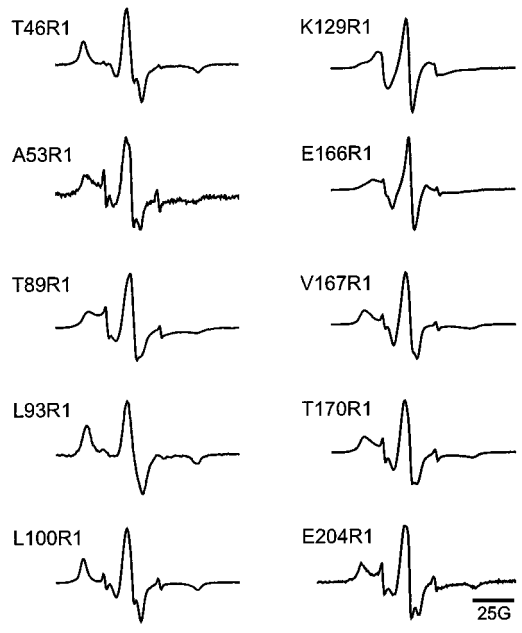

FIGURE 3 Room temperature EPR spectra of the spin-labeled bacteriorhodopsin mutants.

Accessibility to chromium oxalate

The study of the integrity of the spin-labeled bacteriorhodopsin structure was supplemented by measuring the collision frequency of the nitroxide with a freely diffusing paramagnetic probe molecule. The collision frequency of such a probe depends on the product of its translational diffusion coefficient and its local concentration. Molecular oxygen and the water-soluble chromium oxalate (CROX) have been frequently used and found to be ideally suited because of their sizes and solubility properties (Altenbach et al., 1990; Farahbakhsh et al., 1992; Pfeiffer et al., 1999). CROX cannot penetrate into the tightly packed interior of a protein, whereas both the solubility and the diffusion coefficient are high in water. Therefore, the collision frequency between CROX and a spin label side chain that is exposed to the aqueous phase is high. However, the collision frequency should approach zero for spin labels located in the interior of a protein. The application of continuous wave power saturation (Altenbach et al., 1990) yields the accessibility parameter Π (see Methods), which is proportional to the collision frequency of the nitroxide with the paramagnetic reagent. E166R1 and K129R1 are the only residues that reveal considerable values of Π and hence experience collisions with CROX. The respective values, 1.8 and 1.3, are characteristic for nitroxide side chains facing the aqueous phase (Altenbach et al., 1990; Farahbakhsh et al., 1992; Pfeiffer et al., 1999). The values of Π determined for the nitroxides at the other positions are <0.07. Hence, the nitroxide side chains attached to these positions are not accessible to CROX. These findings are in agreement with the structural data (cf. Fig. 2) determined for the wild-type protein.

Hyperfine coupling and polarity profile

Low-temperature EPR spectra were measured at 170 K to restrict molecular motion. In this temperature regime the dynamics of proteins exhibit glasslike behavior, and the reorientational correlation time of an otherwise unrestricted spin label side chain exceeds 100 ns (Steinhoff et al., 1989), i.e., the nitroxides may be considered as completely immo-

bilized on the EPR time scale. However, fast torsional oscillations of very small amplitude of the attached nitroxide are detectable. The residual averaging of the g and hyperfine anisotropy is found to reduce the apparent hyperfine splitting by <2%. At least, this effect contributes to all measurements and will not affect the conclusions, which is based on relative values of the maximum hyperfine splitting $2A_{zz}$. This value was shown to be an ideal measure of the polarity of the nitroxide environment (Griffith et al., 1974). Examples of low-temperature EPR spectra of MTSSL attached to different positions are shown in Fig. 4. Spectral simulations were performed according to the method described by Steinhoff (1988) to yield the g and hyperfine tensor values and the linewidth parameters. As an example, the fit of a simulated spectrum to the experimental data of A53R1 is shown in Fig. 4*a*. The calculated spectra fit the experimental data without any systematic deviations visible. The quality of the simulations and of the experimental data of the other samples is similar, the chi-squared sum (256 B-field values) of the fits to the normalized experimental spectra varies between 0.02 and 0.2, and is essentially determined by the signal-to-noise ratio. The values of A_{zz} determined from different samples of a single mutant were reproducible within a margin of 0.2 G width. The superposition of the spectra obtained for the loop position K129R1 and the internal position L93R1 reveals different hyperfine splittings, $2A_{zz}$, due to environments of different polarity (Fig. 4*b*). The fits yield A_{zz} = 36.5 G for K129R1 and A_{zz} = 34.7 G for L93R1.

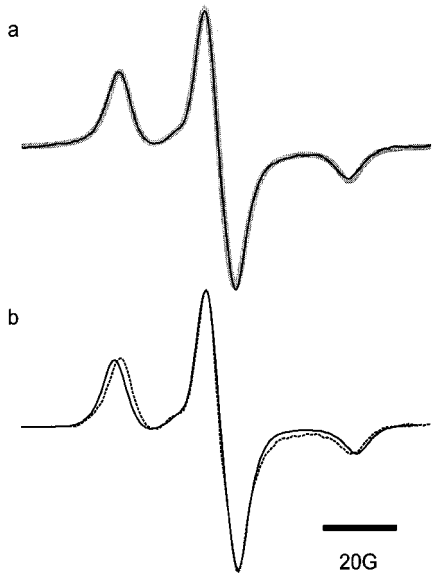

FIGURE 4 (*a*) Experimental (T = 170 K, *thin line*) and simulated (*thick line*) EPR spectra of A53R1. The fitted g and hyperfine tensor values are g_{xx} = 2.0088, g_{yy} = 2.0069, g_{zz} = 2.0027, A_{xx} = 5.4 G, A_{yy} = 5.1G, and A_{zz} = 35.1G. The linewidth was calculated using a superposition of 22% Lorentzian and 78% Gaussian of 4.6 G and 4.0 G width, respectively. (*b*) The superposition of the experimental spectra of K129R1 (*solid line*) and L93R1 (*broken line*) reveals different hyperfine splittings due to different polarities of the nitroxide environment. The fitted values of A_{zz} yield 36.5 G and 34.7 G, respectively.

The A_{zz} values for all samples are plotted in Fig. 5 as a function of the distance, r, from the cytoplasmic surface. The distances were measured from the projections of the C_β positions of the respective residues to a line connecting residues R164, the position of which is arbitrarily set to 0, and G73 on the extracellular surface of the protein. The position of the Schiff base is indicated by an arrow. An error bar of 0.7 nm length indicates the uncertainty of the location of the N-O group in the polarity plot (Fig. 5; for the location of the nitroxide, also cf. Fig. 2).

The largest hyperfine splitting is revealed for E166R1, V167R1, and K129R1. The determined A_{zz} values equal that found for unbound MTS spin label in aqueous solution, which was found to be 36.5 G. According to the molecular model of Grigorieff et al. (1996) residues E166 and V167 are located at the cytoplasmic end of helix F, whereas residue K129 is positioned in the D-E loop on the extracellular surface. The experimental data provide strong evidence that these nitroxides are exposed to the aqueous phase. The high polarity in the environment of residues E166R1 and K129R1 is in agreement with the high mobility of the nitroxide side chains and their high accessibility for CROX. In contrast, the mobility of the side chain of V167R1 is restricted and its accessibility for CROX is low. This agrees with the structural data, which show the side chain of this residue being oriented into the entrance of the CP channel (Essen et al., 1998; Pfeiffer et al., 1999). The polarity of this region is indistinguishable from that of the bulk. However, the environmental polarity of the nitroxides at position 170 and at the end of helix C, position 100, is significantly less. The capability of forming hydrogen bonds between water molecules and the N-O group is restricted for the nitroxides in these locations, which are still close to the water-covered protein surface. The polarity profile decreases along the proton pathway to the Schiff base and exhibits a clear minimum close to position 93 on the cytoplasmic side of the retinal. The polarity is slightly higher at positions 89 and 53 in close vicinity to the retinal

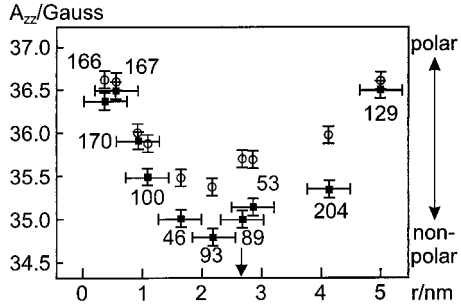

FIGURE 5 The hyperfine tensor element A_{zz} as a function of the nitroxide location with respect to position 164 in absence (*closed squares*) and presence (*open circles*) of azide. The horizontal bars indicated the range of possible locations of the N-O group. For reasons of clarity these bars are omitted for the azide data. The arrow marks the position of the Schiff base. The value of A_{zz} is directly related to the polarity of the nitroxide environment, thus the behavior of the plotted data reflects the hydrophobic barrier in the bacteriorhodopsin proton channel.

and increases again along the proton exit pathway to the bulk.

After addition of 100 mM azide, which increases the ionic strength of the buffer from 0.33 M to 0.36 M, the hyperfine interaction significantly increases for the nitroxides located on both sides of the retinal in the proton channel (cf. Fig. 5), whereas the values found for the nitroxides at the protein surface and at position 170 are unaffected within experimental error. Thus, the increase of the values of A_{zz} of the internal nitroxides that face the proton channel cannot be explained by the increase of ionic strength, because this should influence the external nitroxides to a similar extent. Hence, the observed increase of the hyperfine interaction must be due to changes of the local electrical fields or hydrogen bonding. The affinity constant K_a of azide was determined from the variation of A_{zz} of L93R1 with the azide concentration in the concentration range from 10^{-6} to 1 M. The experimental value, $K_a = (10 \pm 6)$ mM, is in agreement with the value found from the reactivation of the proton transport activity of the D96N mutant, $K_a = 3–4$ mM (Tittor et al., 1989).

DISCUSSION

The g- and A-tensor values of nitroxide spin labels depend on the dielectric susceptibility of the covering solvent and its capability to form hydrogen bonds. Thus, site-directed spin labeling, where a series of spin labels is introduced along the ion pathway, should be ideally suited to study the shape of hydrophobic barriers in ion channels or ion pumps and to reveal a possible change of the hydrogen bond network during the protein function. In this report, spin labels were introduced into bacteriorhodopsin, and the hyperfine interaction was determined from low-temperature EPR spectra in the absence and presence of azide.

Site-directed spin labeling is invasive and the integrity of the BR structure has to be verified by independent methods. The time course of the photocycle is a sensitive measure of structural disturbance. The comparison of the M-decay time of the mutants with that of the wild-type protein reveals that the spin labeling generally allows deprotonation and reprotonation of the Schiff base. Only minor changes of the photocycle compared to the wild type were found for the samples with the spin labels attached to the loops. Here, the interaction between the nitroxide side chain and the protein is weak, as can be judged from the room temperature EPR spectra and consequently, the influence on the protein structure and its function is small. A considerable delay of the recovery of the BR initial state was found for the other mutants. This is pronounced for L93R1 and T170R1. A prolonged O-like intermediate was found for L93R1, in agreement with the results reported by Subramaniam et al. (1997). The decay of intermediate N is delayed for T170R1. The spin-label side chain of T170R1 faces helix G. The nitroxide may thus influence the interaction between helices F and G, which are involved in the structural change during the M-to-N transition (Koch et al., 1991; Subramaniam et al., 1993). This finding is in agreement with results of Brown et al. (1995), who reported a delay of the BR recovery after introduction of maleimide labels at the cytoplasmic end of helix F. The introduction of the nitroxide at positions 53 and 89 in the immediate vicinity of the retinal changes the transition kinetics and the equilibrium between the all-*trans* and 13-*cis*-15-*syn* isomers. Shifts of this equilibrium toward the 13-*cis*-15-*syn* isomer with a simultaneous acceleration of the light-to-dark adaptation was observed in BR at high pressure. This was explained to be due to the smaller volume of the 13-*cis* isomer compared to the all-*trans* isomer (Schulte and Bradley, 1995). The interaction of the nitroxide side chain with the retinal in the mutant T89R1 may act in a similar sense, while that of the nitroxide at position 53 drives the equilibrium toward the all-*trans* isomer. Thus, the mutation and the introduction of spin labels into bacteriorhodopsin may change the photocycle kinetics and the retinal isomer equilibrium, as already known from other site-directed mutagenesis studies (see, e.g., Riesle et al., 1996). However, the mobility of the nitroxide side chains and their accessibility for CROX are in agreement with the structural data of the wild-type protein in all cases. Thus, no evidence for protein unfolding was found. We conclude that the overall structure and function is retained, at least in view of the dielectric properties of the proton channel.

Griffith and co-workers (1974) have shown that the change of the hyperfine interaction (ΔA) of nitroxides caused by solvent perturbation in an isotropic liquid is composed of mainly two terms, $\Delta A = \Delta A_v + \Delta A_h$, where ΔA_v is associated with the electric field contribution due to van der Waals interaction and ΔA_h is the hydrogen bonding term. The authors could show that ΔA_v is related to the dielectric constant of the solvent and that the hydrogen bonding term contributes significantly if the nitroxide is in contact with water or alcohols. For water, e.g., a fraction of 36% of ΔA is due to the dielectric properties, whereas 64% of ΔA is due to hydrogen bonding (Griffith et al. 1974). Thus, the spin label probe is sensitive to changes of the dielectric properties of the environment and, to an even higher extent, to changes of the density and/or strengths of hydrogen bonds.

The EPR spectra of the spin labels attached to positions 166 and 167 at the cytoplasmic end of helix F, and of that bound to K129C at the extracellular surface, reveal a hyperfine splitting identical to that found for MTSSL in frozen glycerol-water glass (cf. Fig. 5). Thus, the dielectric properties of water and the capability of hydrogen bond formation between the nitroxide and water are not altered by the protein in the vicinity of these nitroxide binding sites. The spin label attached to position 170, which does not face the proton channel (Pfeiffer et al., 1999), and that attached to the end of helix C, L100R1, already sense an environment of lower polarity, as can be concluded from the corresponding A_{zz} values. The reorientational motion of these nitroxides is restricted, which shows the intense interaction of the

spin label side chains with neighboring protein atoms. This is evidence for a highly structured environment. Thus, the formation of hydrogen bonds between the N-O group and water may be restricted due to sterical reasons. Additionally, the water density and thus the influence of its high dielectric susceptibility on the hyperfine splitting is reduced at the surface of the protein. The further behavior of the hyperfine splitting reveals a clear minimum near position 93 close to the retinal in the cytoplasmic half of the proton channel. The total variation of A_{zz} from the most polar locations 166, 167, and 129 to the less polar site close to position 93 amounts to 1.7 G. It is useful to compare this value with the A_{zz} variation in microsomal lipid bilayers. Griffith and co-workers (1974) found the lowest hyperfine splitting for nitroxides located within a margin of 2 nm centered around the middle of the hydrated membrane. The corresponding value of A_{zz} differed by 3.3 G from that of a fully hydrated spin label. This is in agreement with A_{zz} values found for MTS spin labels attached to the D helix of BR with the nitroxides facing the lipid phase of a phospholipid bilayer. The value of A_{zz} for the labels attached to positions 116 or 117 close to the middle of the helix yielded 33 G (Altenbach et al., 1994b) compared to 36.5 G found for label positions at the cytoplasmic and extracellular surface. Thus, the difference to the fully hydrated nitroxides amounts to 3.5 G. The total variation of A_{zz} along the proton channel yields only half this value. Hence, the comparably high polarity in the proton channel must be due to the presence of water molecules and of polar or charged groups in the vicinity of the nitroxide. The existence of a hydrogen-bonded network within the proton channel of bacteriorhodopsin has been suggested to facilitate the proton conduction between proton donors and acceptors (Tittor et al., 1989). Water molecules, which should occupy pockets in the proton channel, had been postulated by electron microscopy and molecular dynamics studies (Grigorieff et al., 1996; Bashford and Gerwert, 1992). Neutron diffraction experiments allowed the estimation of a projection of the water density in the membrane plane (Hauss et al., 1997; Weik et al., 1998) and x-ray diffraction experiments could localize bound water molecules in the extracellular and cytoplasmic halves of the proton channel (Pebay-Peyroula et al., 1997; Lücke et al., 1998). Three well defined water molecules could be refined in the extracellular half of the channel, evidence for one or two water molecules could be found in the cytoplasmic half between D96 and the Schiff base (Lücke et al., 1998). From time-resolved FTIR experiments it was concluded that the proton is transferred from the Schiff base to the extracellular surface via an intramolecular hydrogen-bonded network consisting of internal bound water molecules and several residues including R82 and E204 (Rammelsberg et al., 1998). The different polarity profile for the extracellular and cytoplasmic channel halves seen in the present study (cf. Fig. 5) may additionally be explained by the density and position of polar or charged residues. According to the structural data (Pebay-Peyroula et al., 1997; Lücke et al., 1998) five polar or charged residues are located in the vicinity of the cytoplasmic proton pathway, D38, T46, D96, T178, and W182. On the extracellular pathway up to 10 residues may be involved in a hydrogen-bonded network, E9, Y57, R82, D85, T89, Y185, E194, E204, T205, and D212 (Lücke et al., 1998).

The addition of azide does not significantly change the hyperfine splitting of the nitroxides at the protein surface, E166R1, V167R1, and K129R1. Likewise, the polarity in the environment of an internal nitroxide, T170R1, which does not face the proton channel, remains unaffected. However, the polarity in the environment of the internal nitroxides at positions 46, 53, 89, 93, 100, and 204 is significantly increased. Thus, azide affects the proton channel specifically. The changes in both halves of the channel due to the addition of azide are of similar extent, thus retaining the polarity differences between the extracellular and cytoplasmic halves. FTIR spectroscopy data yield evidence for the location of azide close to D85 in the proton release pathway (Le Coutre et al., 1995). Thus azide, although most likely located in the proton release pathway, also affects the properties of the hydrogen-bonded network in the proton uptake pathway. This is in agreement with the observation that both the deprotonation of the Schiff base toward the extracellular surface and its reprotonation from the cytoplasmic surface in mutants with missing proton donors or acceptors (D96N, D85N) are accelerated in the presence of azide (Tittor et al., 1989; 1994; Ganea et al., 1998). Changes of the IR continuum band during the photocycle indicated the existence of a hydrogen-bonded network in the proton uptake pathway of wild-type BR. These changes were found to be absent in the D96N mutant and were restored after addition of azide (Le Coutre et al., 1995). A global effect of azide onto the hydrogen-bonded network of the proton channel is supported by our observation of a decrease of the hydrophobic barrier in both the proton uptake and release pathways.

Proton conduction in proteins is influenced by the rate of protonation and deprotonation reactions, the presence and properties of water, the density and quality of hydrogen bonds and the distribution of charged, polar, and nonpolar residues. These parameters may influence each other and may be additionally modulated by conformational changes that occur during proton translocation. The hyperfine interaction A_{zz} of the spin label is sensitive to the capabilities of forming hydrogen bonds and to the polarizability of the nitroxide environment. Thus, changes of A_{zz} should be correlated to changes of the proton conduction if these two properties are rate-limiting for the proton transfer. The different effect of azide on the rates of the proton uptake in D96N and of the proton release in D85N mutants (Tittor et al., 1989; 1994) shows that additional rate-limiting barriers are involved in the proton transfer process of BR.

The shape of the potential and hydrophobic barrier in ion channels and ion pumps is subject to extensive theoretical studies (Hille, 1992). One crucial requirement for a simulation of potential barriers is the knowledge of reliable experimental data of the polarity within ion channels. The experimental study presented in this report shows that the

combination of site-directed spin labeling and EPR spectroscopy is ideally suited for the collection of the necessary data.

We gratefully acknowledge the support of the Deutsche Forschungsgemeinschaft (SFB 394, C1, C2 to T.R., K.G., and H.-J.S.). D. Oesterhelt is grateful to the Font der Chemischen Industrie.

REFERENCES

Altenbach, C., D. A. Greenhalgh, H. G. Khorana, and W. L. Hubbell. 1994a. A collision gradient method to determine the immersion depth of nitroxides in lipid bilayers: application to spin-labeled mutants of bacteriorhodopsin. *Proc. Natl. Acad. Sci. USA*. 91:1667–1671.

Altenbach, C., T. Marti, H. G. Khorana, and W. L. Hubbell. 1990. Transmembrane protein structure: spin labeling of bacteriorhodopsin mutants. *Science*. 248:1088–1092.

Altenbach, C., H.-J. Steinhoff, D. A. Greenhalgh, G. Khorana, and W. L. Hubbell. 1994b. Factors that determine the EPR spectra of nitroxide side-chains in spin labeled proteins and analysis by molecular dynamics simulation. *Biophys. J.* 66:40*a*. (Abstr.).

Bashford D., and K. Gerwert. 1992. Electrostatic calculations of the pKa values of ionizable groups in bacteriorhodopsin. *J. Mol. Biol.* 224: 473–486.

Brown, L. S., G. Varo, R. Needleman, and J. K. Lanyi. 1995. Functional significance of a protein conformation change at the cytoplasmic end of helix F during the bacteriorhodopsin photocycle. *Biophys. J.* 69: 2103–2111.

Cao, Y., G. Varo, M. Chang, B. F. Ni, R. Needleman, and J. K. Lanyi. 1991. Water is required for proton transfer from aspartate-96 to the bacteriorhodopsin Schiff base. *Biochemistry*. 30:10972–10979.

Earle, K. A., J. K. Moscicki, M. Ge, D. E. Budil, and J. Freed. 1994. 250-GHz electron spin resonance studies of polarity gradients along the aliphatic chains in phospholipid membranes. *Biophys. J.* 66:1213–1221.

Essen, L.-O., R. Siegert, W. D. Lehmann, and D. Oesterhelt. 1998. Lipid patches in membrane protein oligomeres: crystal structure of the bacteriorhodopsin-lipid complex. *Proc. Natl. Acad. Sci. USA*. 95: 11673–11678.

Farahbakhsh, Z. T., C. Altenbach, and W. L. Hubbell. 1992. Spin labeled cysteines as sensors for protein-lipid interaction and conformation in rhodopsin. *Photochem. Photobiol.* 56:1019–1033.

Ferrando, E., U. Schweiger, and D. Oesterhelt. 1993. Homologous bacterio-opsin-encoding gene expression via site-specific vector integration. *Gene*. 125:41–47.

Ganea, C., J. Tittor, E. Bamberg, and D. Oesterhelt. 1998. Chloride- and pH-dependent proton transport by BR mutant D85N. *Biochim. Biophys. Acta*. 1368:84–96.

Griffith, O. H., P. J. Dehlinger, and S. P. Van. 1974. Shape of the hydrophobic barrier of phospholipid bilayers (evidence for water penetration in biological membranes). *J. Membr. Biol.* 15:159–192.

Grigorieff, N., T. A. Ceska, K. H. Downing, J. M. Baldwin, and R. Henderson. 1996. Electron-crystallographic refinement of the structure of bacteriorhodopsin. *J. Mol. Biol.* 259:393–421.

Hatanaka, M., H. Kandori, and A. Maesa. 1997. Localization and orientation of functional water molecules in bacteriorhodopsin as revealed by polarized Fourier transform infrared spectroscopy. *Biophys. J.* 73: 1001–1006.

Hauss, T. H., G. Papadopoulos, S. A. W. Verclas, G. Büldt, and N. A. Dencher. 1997. Neutron diffraction on purple membranes. Essential water molecules in the light-driven proton pump bacteriorhodopsin. *Physica B.* 234:217–219.

Hessling, B., G. Souvignier, and K. Gerwert. 1993. A model-independent approach to assigning bacteriorhodopsin's intramolecular reactions to photocycle intermediates. *Biophys. J.* 65:1929–1941.

Hille, B. 1992. Ionic channels of excitable membranes, 2nd ed. Sinauer Associates, Sunderland, MA.

Hubbell, W. L., and C. Altenbach. 1994. Investigation of structure and dynamics in membrane proteins using site-directed spin labeling. *Curr. Opin. Struct. Biol.* 4:566–573.

Hubbell, W. L., H. S. Mchaourab, C. Altenbach, and M. A. Lietzow. 1996. Watching proteins move using site-directed spin labeling. *Structure*. 4:779–783.

Kimura, Y., D. G. Vassylyev, A. Miyazawa, A. Kidera, M. Matsushima, K. Mitsuoka, K. Murata, T. Hirai, and Y. Fujiyoshi. 1997. Surface of bacteriorhodopsin revealed by high-resolution electron crystallography. *Nature*. 389:206–211.

Koch, M. H. J., N. A. Dencher, D. Oesterhelt, H.-J. Plön, G. Rapp, and G. Büldt. 1991. Time-resolved x-ray diffraction study of structural changes associated with the photocycle of bacteriorhodopsin. *EMBO J.* 10: 521–526.

Lam, W. L., and W. F. Doolittle. 1989. Shuttle vectors for the archaebacterium *Halobacterium volcanii. Proc. Natl. Acad. Sci. USA*. 86: 5478–5482.

Lanyi, J. K. 1993. Proton translocation mechanism and energetics in the light-driven pump bacteriorhodopsin. *Biochim. Biophys. Acta*. 1183: 241–261.

Le Coutre, J., J. Tittor, D. Oesterhelt, and K. Gerwert. 1995. Experimental evidence for hydrogen-bonded network proton transfer in bacteriorhodopsin shown by Fourier-transform infrared spectroscopy using azide as catalyst. *Proc. Natl. Acad. Sci. USA*. 92:4962–4966.

Lücke, H., H.-T. Richter, and J. K. Lanyi. 1998. Proton transfer pathways in bacteriorhodopsin at 2.3 angstrom resolution. *Science*. 280: 1934–1937.

Mchaourab, H. S., M. A. Lietzow, K. Hideg, and W. L. Hubbell. 1996. Motion of spin-labeled side chains in T4 lysozyme. Correlation with protein structure and dynamics. *Biochemistry*. 35:7692–7704.

Oesterhelt, D. 1998. Structure and mechanism of the family of retinal proteins from halophilic archaea. *Curr. Opin. Struct. Biol.* 8:489–500.

Oesterhelt, D., M. Meentzen, and L. Schuhmann. 1973. Reversible dissociation of the purple complex in bacteriorhodopsin and identification of 13-*cis* and all-*trans*-retinal as its chromophore. *Eur. J. Biochem.* 40: 453–463.

Oesterhelt, D., and W. Stoeckenius. 1974. Isolation of the cell membrane of *Halobacterium halobium* and its fraction into red and purple membrane. *Methods Enzymol.* 31:667–686.

Pebay-Peyroula, E., G. Rummel, J. P. Rosenbusch, and E. M. Landau. 1997. X-ray structure of bacteriorhodopsin at 2.5 angstroms from microcrystals grown in lipidic cubic phases. *Science*. 277:1676–1681.

Pfeiffer, M., T. Rink, K. Gerwert, D. Oesterhelt, and H.-J. Steinhoff. 1999. Site-directed spin labeling reveals the orientation of the amino acid side chains in the E-F loop of bacteriorhodopsin, *J. Mol. Biol.* 287:163–172.

Rammelsberg, R., G. Huhn, M. Lübben, and K. Gerwert. 1998. Bacteriorhodopsin's intramolecular proton-release pathway consists of a hydrogen-bonded network. *Biochemistry*. 37:5001–5009.

Riesle, J., D. Oesterhelt, N. A. Dencher, and J. Heberle. 1996. D38 is an essential part of the proton translocation pathway in bacteriorhodopsin. *J. Biol. Chem.* 35:6635–6643.

Rink, T., J. Riesle, D. Oesterhelt, K. Gerwert, and H.-J. Steinhoff. 1997. Spin labeling studies of the conformational changes in the vicinity of D36, D38, T46, and E161 of bacteriorhodopsin during the photocycle. *Biophys. J.* 73:983–993.

Schulte, A., and L. Bradley II. 1995. High-pressure near-infrared Raman spectroscopy of bacteriorhodopsin light to dark adaptation. *Biophys. J.* 69:1554–1562.

Schweiger, U. 1996. Funktionelle Charakterisierung der Retinalbindungstasche von Bakteriorhodopsin durch spezifische Mutangenese. Ph.D. thesis, Leopold-Franzens-Universität, Innsbruck, Austria.

Steinhoff, H.-J. 1988. A simple method for determination of rotational correlation times and separation between rotational and polarity effects from EPR spectra of spin labeled biomolecules in a wide correlation time range. *J. Biochem. Biophys. Meth.* 17:237–248.

Steinhoff, H.-J., and W. L. Hubbell. 1996. Calculation of electron paramagnetic resonance spectra from Brownian dynamics trajectories: application to nitroxide side chains in proteins. *Biophys. J.* 71:2201–2212.

Steinhoff, H.-J., K. Lieutenant, and J. Schlitter. 1989. Residual motion of hemoglobin-bound spin labels as a probe for protein dynamics. *Z. Naturforsch.* 44c:38–46.

Steinhoff, H.-J., R. Mollaaghababa, C. Altenbach, K. Hideg, M. Krebs, H. G. Khorana, and W. L. Hubbell. 1994. Time-resolved detection of structural changes during the photocycle of spin-labeled bacteriorhodopsin. *Science*. 266:105–107.

Subramaniam, S., M. Gerstein, D. Oesterhelt, and R. Henderson. 1993. Electron diffraction analysis of structural changes in the photocycle of bacteriorhodopsin. *EMBO J.* 12:1–8.

Subramaniam, S., A. R. Faruqi, D. Oesterhelt, and R. Henderson. 1997. Electron diffraction studies of light-induced conformational changes in the Leu-93 → Ala bacteriorhodopsin mutant. *Proc. Natl. Acad. Sci. USA*. 94:1767–1772.

Tittor, J., C. Soell, D. Oesterhelt, H.-J. Butt, and E. Bamberg. 1989. A defective proton pump, point-mutated bacteriorhodopsin Asp96-Asn is fully reactivated by azide. *EMBO J.* 8:3477–3482.

Tittor, J., M. Wahl, U. Schweiger, and D. Oesterhelt. 1994. Specific acceleration of de- and reprotonation steps by azide in mutated bacteriorhodopsins. *Biochim. Biophys. Acta*. 1187:191–197.

Varo, G., and J. K. Lanyi. 1991. Thermodynamics and energy coupling in the bacteriorhodopsin photocycle. *Biochemistry*. 30:5016–5022.

Weik, M., G. Zaccai, N. A. Dencher, D. Oesterhelt, and T. Hauss. 1998. Structure and hydration of the M-state of the bacteriorhodopsin mutant D96N studied by neutron diffraction. *J. Mol. Biol.* 275:625–634.

Wikström, M. 1998. Proton translocation by bacteriorhodopsin and heme-copper oxidases. *Curr. Opin. Struct. Biol.* 8:480–488.